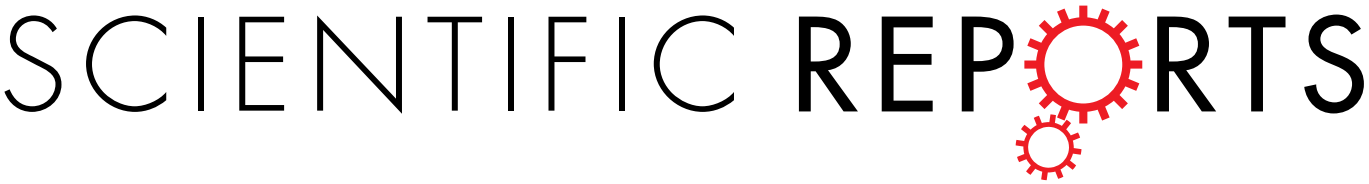

OPEN

Received: 02 July 2015
Accepted: 21 December 2015
Published: 28 January 2016

Wind-blown Sand Electrification Inspired Triboelectric Energy Harvesting Based on Homogeneous Inorganic Materials Contact: A Theoretical Study and Prediction

Wenwen Hu[1], Weiwei Wu[2,3] & Hao-miao Zhou[1]

Triboelectric nanogenerator (TENG) based on contact electrification between heterogeneous materials has been widely studied. Inspired from wind-blown sand electrification, we design a novel kind of TENG based on size dependent electrification using homogeneous inorganic materials. Based on the asymmetric contact theory between homogeneous material surfaces, a calculation of surface charge density has been carried out. Furthermore, the theoretical output of homogeneous material based TENG has been simulated. Therefore, this work may pave the way of fabricating TENG without the limitation of static sequence.

In the earth's crust, silicon is the second most abundant element and various forms of silica is the most common composition unit of sand. For wind-blown sand granular systems, such as dust devil, sand storm, wind-blown sand saltation, etc, the upward electric field phenomenon originated from the positively charged large particles saltate/creep near the surface and small negatively charged smaller particles suspend into the air is widely observed[1]. The charged wind-blown sand granular systems always cause various damages, especially to the attenuation of electromagnetic wave signals caused by the light scattering and absorption of wind-blown sand&dust[2]. Nowadays, people reluctantly seem this huge static electric energy in those systems as harmful and waste energy and suffers their damages. However, an interesting and desired topic, how to take advantage of this natural phenomenon and convert the tremendous, harmful energy to useful electricity, hasn't been paid enough attention and is a lack of study.

Based on different physical rules including electromagnetic induction effect[3], electrostatic effect[4], piezoelectric effect[5] and so on, human beings convert mechanical energy to electricity that is one of the main kind of power source. Since 2012, triboelectric nanogenerator (TENG) has been invented as a novel technology to harvest waste mechanical energy which is a possible solution of not only portable electronics but also the energy crisis for human beings[6]. Comparing with piezoelectric materials based nanogenerator, TENG represents some unique merits such as high conversion efficiency, low fabrication cost, reliable robustness, which attaches great research interests both on theoretical and experimental studies[7–13].

Generally, the working principle of TENG includes two processes[9,14]. First, two different kinds of materials located at different sites of electrostatic sequence obtain opposite charges on the surface via contact electrification with or without rubbing. Second, the electrodes made of oppositely charged materials move to change the capacitance for creating an electric potential difference that drives the free electrons in the external circuit to flow back and forth as alternating current (AC). Both in contact and sliding mode, the electrification between two different materials is a key step for generating electricity[12,15,16]. Till now, TENGs have been developed by assembling two different kinds of materials with the empirical arrangement in the static sequence, for example, PET and Kapton[6], PTFE and Al[17], PDMS and Al[18], PMMA and Kapton[19], PDMS and ITO[20], TiO_2 and PTFE[21], PDMS and Au[22],

[1]College of Information Engineering, China Jiliang University, Hangzhou, 310018, PRC. [2]College of Materials and Textiles, Key Laboratory of Advanced Textile Materials and Manufacturing Technology of the Ministry of Education, Zhejiang Sci-Tech University, 310018, PRC. [3]Department of Chemical Engineering & Russell Berrie Nanotechnology Institute, Technion – Israel Institute of Technology, Haifa, 3200003, Israel. Correspondence and requests for materials should be addressed to W.H. (email: huwenw03@gmail.com)

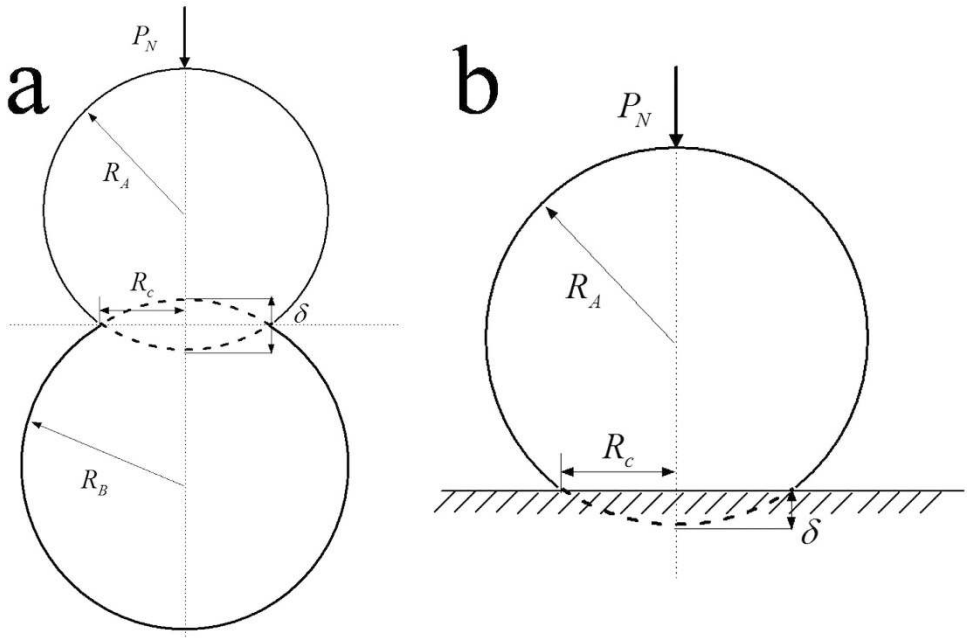

Figure 1. Scheme of the contact of a sphere with radius R_A on (**a**) another sphere with radius R_B; (**b**) a rigid flat object under a normal point load P_N. δ is the overlapped deformation, and R_c is the contact radius.

PVDF and nylon[23], etc. With the limitation of static sequence, almost either of these two kinds of materials is polymer. Contact electrification occurs not only between heterogeneous but also homogeneous materials, which has been demonstrated by several experimental works, such as silica-silica[24–29], aluminum oxide-aluminum oxide[25], polymer-polymer[30–32]. Some homogeneous materials based TENGs also have promising performance[33]. Although polymer is always cheap, flexible and light, polymer based TENG is highly unfavorable to work in harsh environment such as desert, outer space and so on for its narrow working temperature area, fast aging and poor antiwear property[34]. Therefore, it is valuable to design and develop a new kind of TENG made with total inorganic materials like silica-silica to work in special environment.

For the electrification between identical materials, high energy trapped surface states theory proposed by Lowell and Truscutt[35] has been widely used to explain charge transfer during asymmetric rubbing[26,36,37] Based on high energy trapped states theory, particle-size-dependent charging, such as larger particles tends to be positively charged and smaller particles tends to be negatively charged, has been well explained[26,28,36–38]. In the wind-blown sand granular system, mechanisms of size-dependent electrification between identical insulator particles have been widely studied[16,26,36–40], such as asymmetric contact between two particles with transfer of high-energy trapped electrons[37] or holes[26] (HETH). In our previous work, a contact charge model of high-energy trapped holes has been developed[26] and verified with experiments[24,26] for collision of homogeneous silica particles to predict the size-dependent contact electrification. From the experimental point view, silica film, made with earth abundant element oxygen and silicon, is chemical inertia and compatible with many semiconductor fabrication process like thermal oxidation[41], magnetron sputtering[42], sol-gel coating[43], plasma enhanced chemical vapor deposition[44], atom layer deposition[45] and so on. Meanwhile, the synthesis of silica nanoparticles is also widely studied for many years[46]. Therefore, inspired by these natural phenomenon and studies, using homogenous silica based materials with different sizes as the contact electrification layer to fabricate TENG for energy harvesting, is highly feasible, which may pave a new way to develop a novel kind of TENG working in harsh environment.

In this manuscript, we propose a new kind of TENG based on contact electrification between homogeneous silica materials with different sizes for harvesting energy. A comprehensive theoretical model is established to understand the effect of size dependent elasticity on the surface charge density of chemically identical silica nanoparticles under normal loads. To our best knowledge, it is the first time of calculating the surface charge density after single time contact electrification for TENG through theoretical simulation. Then, these results are applied to predict the output characteristics of the contact-mode and sliding-mode TENGs. We demonstrate that the maximum output power of TENG using earth abundant and identical silica as contact electrification layer will reach 12.98 μW and 13.92 nW in contact and sliding model respectively. Indeed, the output will be greatly enhanced after multi-times contact electrification for more accumulated charges and higher surface charge density[30,47] Furthermore, the whole TENG is covered with homogenous materials (silica), which may broaden the application of TENG in harsh environment.

Results

Denote two neutrally-charged sphere particles, A and B with radii R_A and R_B respectively, in a normally elastic colliding process, as shown in Fig. 1(a). Based on high-energy trapped hole contact charging model[26], the net

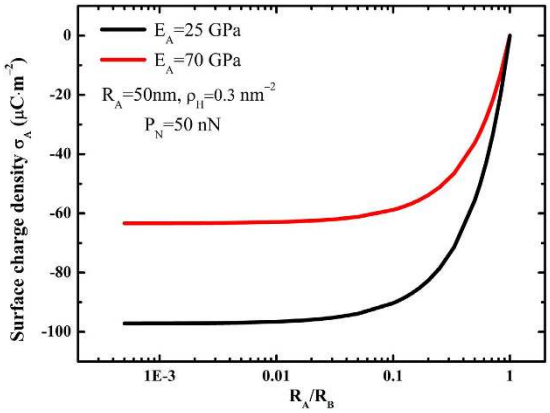

Figure 2. For Hertzian contact of two spheres under normal load $P_N = 50$ nN, the surface charge density σ_A of sphere R_A varies with the radii ratio R_A/R_B.

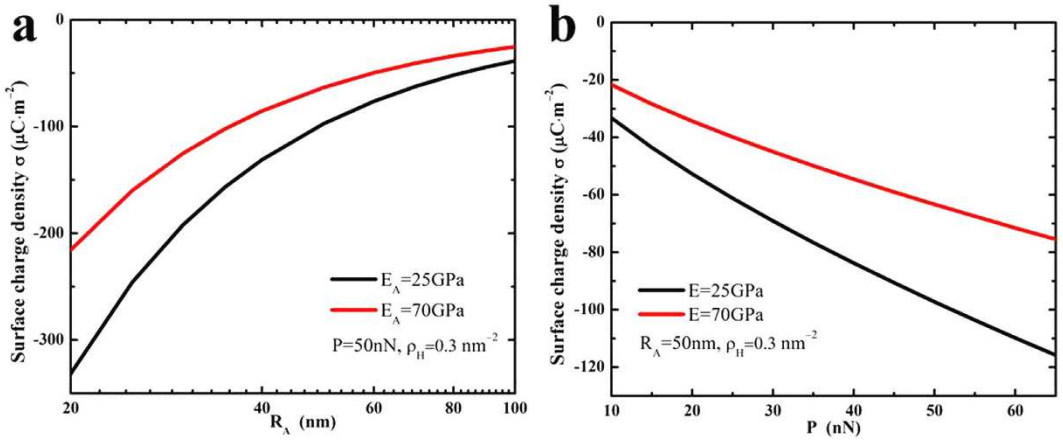

Figure 3. For Hertzian contact between a sphere and a plate, the surface charge density σ_A varies with (a) radius R_A under normal point load $P_N = 50$ nN; and (**b**) normal point load P with $R_A = 50$ nm.

charge transfer of particle *A*equals to the number of high-energy trapped holes gained from particle *B* to particle *A* subtracting that lost from particle *A* to particle *B*, that is,

$$\Delta q_A = e\rho_H S_B - e\rho_H S_A, \tag{1}$$

where S_i is the surface area of the contact part of sphere particle i ($i = A, B$), e is the elementary charge, $\rho_H(m^{-2})$ is the surface density of the high-energy trapped holes which is assumed to be identical for all particles initially[26,37] The net charge transfer Δq_B of particle *B* equals to $-\Delta q_A$.When $R_B \to \infty$, Hertzian normal contact of two spheres will become the contact between a sphere and a rigid flat, as shown in Fig. 1(b). If the contact surface radius $R_c$is given, the surface area of the contact part S_i of sphere *i* can be predicted,

$$S_i = 2\pi R_i^2 \left(1 - \frac{\sqrt{R_i^2 - R_c^2}}{R_i}\right). \tag{2}$$

The net charge transfer of normal contact spheres is determined by the difference of surface areas of contact part $(S_B - S_A)$. Let $R_A < R_B$, the contacted surface area S_A will be greater than the contacted surface area S_B, and then the net charge transfer $\Delta q_B > 0$ and $\Delta q_A < 0$. If pre-collisional particles are both neutrally charged, the larger particle tends to be positively charged and the smaller particle tends to be negatively charged.

In order to achieve an optimal design of TENGs, the surface charge density is a vital parameter determining the output characteristics. When R_A is fixed, Fig. 2 shows that the surface charge density $\sigma_A = \Delta q_A / S_A$ of the post-collisional particle *A* decreases with radius R_B (or increases with $1/R_B$) and finally reaches its minimum value while $R_B \to \infty$ (or $1/R_B \to 0$). When the radius R_B tends to infinite, the particle-particle Hertzian contact can be treated as the particle-plane contact, and in such case the surface charge density tends to its extreme value.

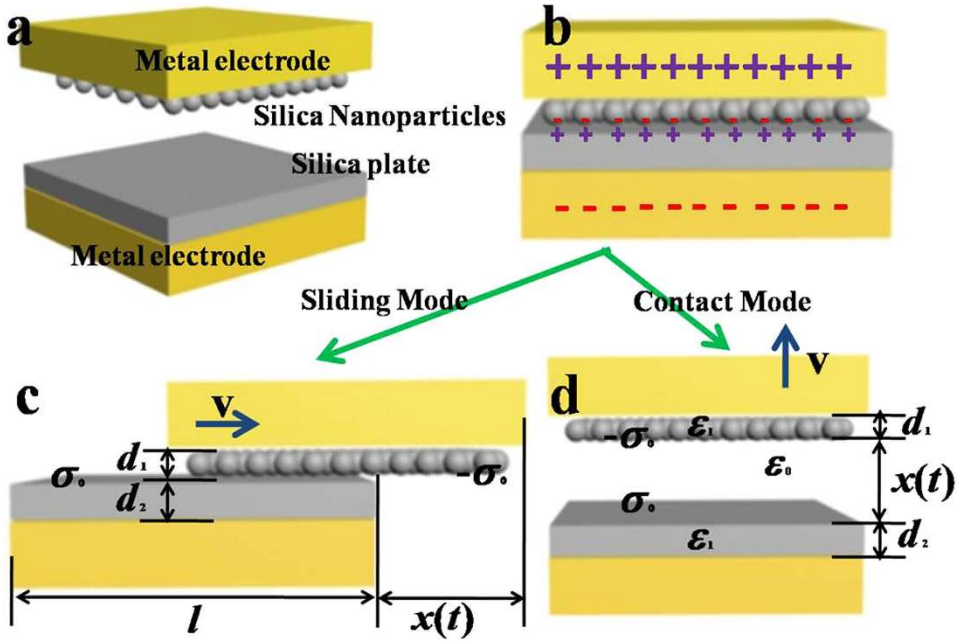

Figure 4. Scheme of (**a**) contact-mode and (**b**) sliding-mode TENGs. The top surface is decorated with SiO_2 nanoparticles, and the bottom surface is flat SiO_2 plate. After separation, the bottom surface has the surface charge density σ_0 and the top surface the surface charge density $-\sigma_0$.

Therefore the particle-plane Hertzian contact case will be an optimal design to obtain the maximum charge & power outputs for TENGs.

In the case of elastic particle-plane Hertzian contact, we predict the surface charge density σ_A varying with the normal load P and the radius R_A, as shown in Fig. 3. The absolute value of the surface charge density, $|\sigma_A|$, increases with the normal load P increasing, but decreases with the increase of the radius R_A.

Materials reduced to submicron or/and nanoscale show different mechanical properties compared to what they show on macroscale. Wang *et al.*[48] pointed out that the Young's module of silica nanowires of 100 nm diameter SiO_2 nanowires is much lower than that of bulk SiO_2 materials. Since the Young's module reveals the strain-stress relationship, it will have an impact on the contact area of Hertzian contact and also on the contact charge. Figures 2 and 3 demonstrate that the Young's module have significant effects on the surface charge density. For instance, as shown in Fig. 2, when $E_A = 25$ GPa, the absolute value of the extreme surface charge density, will be 53.5% greater than the case $E_A = 70$ GPa, respectively. Therefore, in this study we consider the nanoscale effect and take the Young's module as 25 GPa.

Instead of taking advantage of contact electrification between different insulators[6,17–23], we choose the identical silica insulators with the property of size-dependent polarity during contact electrification. Figure 4 shows the schemes of contact-mode and sliding-mode TENGs. The top surface is decorated with a layer of SiO_2 nanoparticles, and the bottom surface is flat SiO_2 plate. Thin layers of metal film are deposited on two SiO_2 material plates as the metal electrodes. The metal electrodes in the upper and lower plates are called the top and down electrodes, respectively.

Figure 4(a) is the schematic diagram of the structure of our TENG containing two metal electrodes, silica nanoparticle and silica plate. Initially, the two surfaces are neutrally charged. As observed in wind-blown sand granular systems and our previous work, the surface coated with SiO_2 nanoparticles will be negatively charged and the SiO_2 plane surface will be positively charged after single time contacting[26], and the bottom surface has the surface charge density σ_0 and the top surface the surface charge density $-\sigma_0$as shown in Fig. 4(b–d) are the schematic diagrams of sliding and contact mode separately. After separation, the electric charge of a single SiO_2 nanoparticle will be

$$q_{grain} = -\pi e \rho_H [R_c^2 - 2R_A^2 + 2R_A\sqrt{R_A^2 - R_c^2}] \tag{3}$$

If there are N particles decorated on a plane with the surface area $S(S = wl, l$: length; w: width), the number density will be $n = N/S$. After separation of two planes, the total electric charge of nanoparticle-decorated top plane will be,

$$q_{top} = -N\pi e \rho_H [R_c^2 - 2R_A^2 + 2R_A\sqrt{R_A^2 - R_c^2}] \tag{4}$$

And the averaged surface charge density of the down plane σ_0 will be

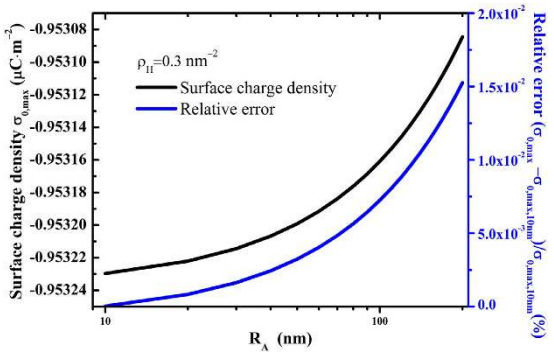

Figure 5. For a square surface fully decorated with nanoparticles, the maximum surface charge density $\sigma_{0,\,max}$ varies with the radius R_A.

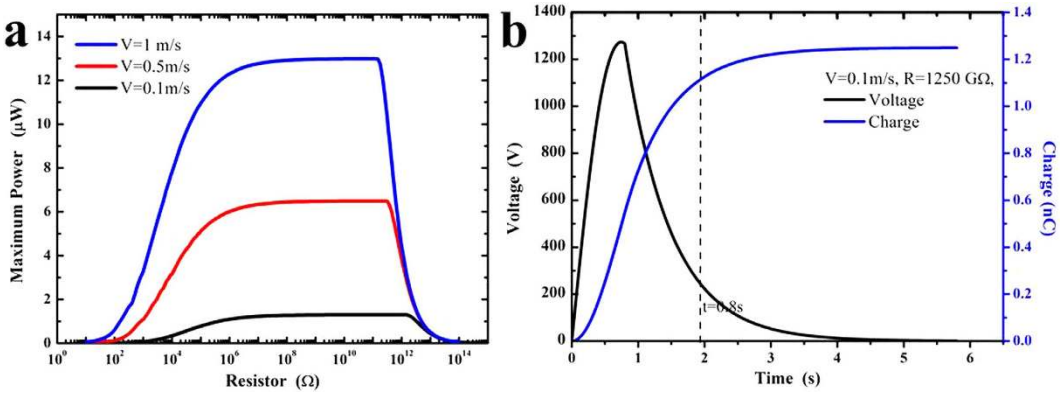

Figure 6. Outputs of contact-mode TENGs with uniform velocity of separation. (**a**) Maximum power outputs vary with resistance; (**b**) Under the optimum power output (R = 1250 GΩ, v = 0.1 m/s), voltage & charge output profiles change with time.

$$\sigma_0 = n\pi e\rho_H[R_c^2 - 2R_A^2 + 2R_A\sqrt{R_A^2 - R_c^2}] \tag{5}$$

Then, the averaged surface charge density of the top plane will be $-\sigma_0$. For a rectangle plane with length l and width w, the maximum number of particles coated on such surface will be N_1N_2, where N_1 and N_2 can be solved by $N_1R_A \le l/2 < R_A(N_1+1)$ and $N_2R_A \le w/2 < (N_2+1)R_A$, respectively. Noticeably, the surface charge density σ_0 increases with n, and the maximum surface charge density$\sigma_{0,\,max}$ will be $N_1N_2\pi e\rho_H[R_{c,\,max}^2 - 2R_A^2 + 2R_A\sqrt{R_A^2 - R_{c,\,max}^2}]/wl$, where $R_{c,\,max}$ denotes the maximum elastic contact surface radius which can be solved according to the critical normal load. For a square surface, $N_1N_2/wl \to 1/4R_A^2$, and the maximum surface charge density $\sigma_{0,\,max}$tends to be $\pi e\rho_H[R_{c,\,max}^2 - 2R_A^2 + 2R_A\sqrt{R_A^2 - R_{c,\,max}^2}]/4R_A^2$. For instance, when $R_A = 10$ nm,the maximum surface charge density. Figure 5 shows that$\sigma_{0,\,max}$ slightly increase linearly with R_A and is nearly a constant value $-0.953\,\mu C\,m^{-2}$ with R_A in the range 10 ~ 100 nm, and the relative error$|(\sigma_{0,\,max} - \sigma_{0,\,max,10nm})/\sigma_{0,\,max,10nm}|$ is very small. The above maximum surface charge density means that particles are densely distributed, and this is an ideal state. While in this ideal state, the squeezing action between a particle and its adjacent particles under external forces also affects the Hertzian deformation of particle-plane contact. In order to avoid such inter-particle effects, sparse distribution of nanoparticles is more reasonable. For example, when a quarter of the maximum number of particles such as $N_1N_2/4$ are decorated on the top surface, the surface charge density will be $\sigma_0 = \sigma_{0,\,max}/4 = 0.238\ \mu C \cdot m^{-2}$.

For normal contact-mode and sliding-mode TENGs connected to an arbitrary resistor$R$, the output properties have been respectively discussed[14,49]. Figures 6 and 7 respectively depicts the theoretical output properties of normal contact-model and sliding-mode of TENGs. The parameters of our TENGs are given in Table 1. For instance, the width $w = 50$ mm, the length $l = 100$ mm, the thicknesses $d_1 = 2R_A = 100$ nm, and $d_2 = 100\ \mu m$ for both contact-mode and sliding-mode TENGs. The maximum departing distance of contact-mode TENGs is 80mm, and the maximum sliding distance d_{max} of sliding-mode TENGs is also 80mm. When the velocities are respectively 0.1 m/s, 0.5 m/s, 1 m/s, theoretical calculations of maximum power outputs are carried out with different resistances, as shown in Figs 6(a) and 7(a). Obviously, there will be optimum values of resistance R for contact model and sliding-mode[14,49]. For instance, as shown in Fig. 6(a), when the power outputs reach their

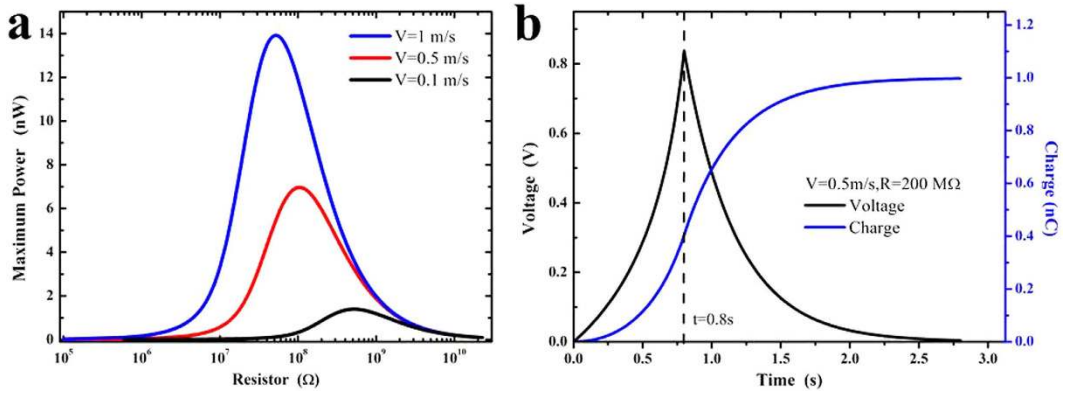

Figure 7. Outputs of sliding-mode TENGs with uniform velocity of separation. (**a**) Maximum power outputs vary with resistance; (**b**) Under the optimum power output (R = 200 MΩ, v = 0.5 m/s), voltage & charge output profiles change with time.

Radius of SiO2 particle	$R_A = 50$ nm
Dielectric of SiO_2 & Thickness	$\varepsilon_1 = 3.9$, $d_1 = 100$ nm, $d_2 = 100\mu$m
Width & Length	$w = 50$mm, $l = 100$mm,
Velocity	$v = 0.1, 0.5, 1$ m/s
Maximum distance	$x_{max} = 80$mm, $d_{max} = 80$ mm
Poison ratio	$\nu_A = \nu_B = 0.3$
Young's module	$E_A = 25$ GPa, $E_B = 70$GPa
Yield strength	$\sigma_Y = 80$ MPa
Surface density of HETHs	$\rho_H = 0.3\,nm^{-2}$

Table 1. Parameters.

optimum values 1.298 μW, 6.491 μW and 12.98 μW after single time contact electrification for contact-model TENGs, the resistances are respectively 1250 GΩ (separating velocity is 0.1 m/s), 275 GΩ (separating velocity is 0.5m/s), and 125 GΩ (separating velocity is 1 m/s). For sliding-model TENGs, the maximum power output could reach 13.92 nW after single time electrification when sliding velocity is 1 m/s. According to optimization of resistance value, Figs 6(b) and 7(b) respectively demonstrate the voltage and charge outputs of contact-model TENGs and sliding-mode TENGs when separating & sliding velocities are both 0.1m/s. Therefore, our optimized designs of contact-mode and sliding-mode TENGs based on contact electrification of homogeneous materials with different sizes would provide a new way for harvesting natural wind-blown energy to drive the nano/micro scale instruments.

Discussion

Inspired from wind-blown sand electrification, we design a novel kind of TENG based on size dependent electrification using identical silica materials for harvesting energy. A theoretical mode is established to elucidate the mechanism of the contact electrification process and a calculation of surface charge density has been carried out. Furthermore, the output of homogeneous material based TENG has been simulated. We demonstrate that the maximum power outputs of TENG using earth abundant and homogenous silica as contact electrification layer will reach 12.98 μW and 13.92 nW in contact and sliding model after single time contact electrification, respectively. Indeed, the output will be greatly enhanced after multi-times contact electrification for more accumulated charges and higher surface charge density. The design of our TENG is polymer free and breaks the limitation of static sequence, which may broaden the application of TENG in harsh environment.

Method

The high-energy trapped hole contact charging model[26] is used to predict the net charge transfer and the surface charge density when identical SiO_2 particle-particle or particle-plane contact. The net charge transfer is related to the Hertzian contact area.

According to Hertzian normal contact theory, each sphere will undergo a normal deflection and a contact surface when the two spheres are subjected to a normal load$P$, as shown in Fig. 1(a). And the normal deflection δ is given by,

$$\delta = \left(\frac{9P^2}{16RK^2}\right)^{\frac{1}{3}}, \tag{6}$$

where K is a material constant and commonly referred to as the effective stiffness,

$$\frac{1}{K} = \frac{1-\nu_A^2}{E_A} + \frac{1-\nu_B^2}{E_B}, \tag{7}$$

where E_A, E_A are the Young's modules and ν_A, ν_B are the Poisson's ratios, respectively. The effective radius of curvature R of the two spheres is defined as,

$$\frac{1}{R} = \frac{1}{R_A} + \frac{1}{R_B}, \tag{8}$$

where R_i is the radius of sphere i ($i = A,\ B$).When $R_B \to \infty$, Hertzian normal contact of two spheres will become the contact of a sphere and a rigid flat, as shown in Fig. 1(b). The contact surface radius R_c and the normal deflection δ satisfy $R_c^2 = R\delta$, and thus the contact surface radius R_c will be,

$$R_c = \left(\frac{3PR}{4K}\right)^{\frac{1}{3}} \tag{9}$$

Here, we only consider the elastic Hertzian contact; therefore we need to calculate the critical normal load P_c from elastic stage to plastic stage. Love *et al.* demonstrated the stress produced in a semi-infinite body[50],

$$\sigma_r = \frac{3P}{2\pi {R_c}^2}\left\{\frac{1-2\upsilon}{3}\frac{{R_c}^2}{r^2}\left[1-\left(\frac{z}{\sqrt{\lambda}}\right)^3\right] + \frac{z(1+\upsilon)}{a}\tan^{-1}\frac{R_c}{\sqrt{\lambda}} + \frac{z\sqrt{\lambda}(1-\upsilon)}{{R_c}^2+\lambda} - \frac{2z}{\sqrt{\lambda}} + \frac{{R_c}^2 z^3}{\sqrt{\lambda}(\lambda^2+{R_c}^2 z^2)}\right\}, \tag{10}$$

$$\sigma_r = \frac{3P}{2\pi {R_c}^2}\left\{-\frac{1-2\upsilon}{3}\frac{{R_c}^2}{r^2}\left[1-\left(\frac{z}{\sqrt{\lambda}}\right)^3\right] + \frac{z(1+\upsilon)}{a}\tan^{-1}\frac{R_c}{\sqrt{\lambda}} - \frac{z\sqrt{\lambda}(1-\upsilon)}{{R_c}^2+\lambda} - \frac{2\upsilon z}{\sqrt{\lambda}}\right\}, \tag{11}$$

$$\sigma_z = -\frac{3P}{2\pi}\frac{z^3}{\sqrt{\lambda}(\lambda^2+{R_c}^2 z^2)}, \tag{12}$$

$$\tau_{rz} = -\frac{3P}{2\pi}\frac{rz^3\sqrt{\lambda}}{(\lambda+{R_c}^2)(\lambda^2+{R_c}^2 z^2)}, \tag{13}$$

where $2\lambda = r^2 + z^2 - {R_c}^2 + \sqrt{\left(r^2+z^2-{R_c}^2\right)^2 + 4z^2{R_c}^2}$. Under normal point load, the plastic deformation starts at the contact area, and the initially yielding point will be on the axis of z of the elastic semi-infinite body. When $r \to 0$, the stress at points on the axis of z will be

$$\sigma_r = -\frac{3P}{2\pi {R_c}^2}\left\{(1+\upsilon)\left(1-\frac{z}{a}\tan^{-1}\frac{R_c}{z}\right) - \frac{{R_c}^2}{2({R_c}^2+z^2)}\right\}, \tag{14}$$

$$\sigma_\theta = -\frac{3P}{2\pi {R_c}^2}\left\{(1+\upsilon)\left(1-\frac{z}{a}\tan^{-1}\frac{R_c}{z}\right) - \frac{{R_c}^2}{2({R_c}^2+z^2)}\right\}, \tag{15}$$

$$\sigma_z = -\frac{3P}{2\pi}\frac{1}{({R_c}^2+{R_c}^2 z^2)}, \tag{16}$$

$$\tau_{rz} = 0. \tag{17}$$

Here, J_2, the second invariant of stress deviator tensor is applied to predicted the critical normal load, and $J_2 = \frac{1}{3}(\sigma_r - \sigma_z)^2$. According to the Von Mises criteria, the yielding function $f_0 = J_2 - \frac{{\sigma_Y}^2}{3} = 0$ for axial extension experiments, where σ_Y is the yield strength. Therefore, the critical normal point load can be derived by solving function $|\sigma_r - \sigma_z| = \sigma_Y$.

Finally, we carry out a theoretical study and prediction of wind-blown sand electrification inspired triboelectric energy harvesting based on homogeneous inorganic materials contact. For normal contact-mode and sliding-mode TENGs connected to an arbitrary resistor R, the charges on the top electrode as a function of time are respectively given as[14,49],

$$Q_{contact}(t) = \sigma_0 S - \sigma_0 S e^{-f(t)} - \frac{\sigma_0(d_1 + d_2)}{R\varepsilon_0\varepsilon_1} e^{-f(t)} \cdot \int_0^t e^{f(\tau)} d\tau, \tag{18}$$

$$Q_{sliding}(t) = e^{\int A(t)dt}\left[\int B(t) e^{-\int A(t)dt} dt + C_0\right], \tag{19}$$

where $f(t) = \frac{1}{RS\varepsilon_0}\left(\frac{(d_1+d_2)t}{\varepsilon_1} + \int_0^t x(t)dt\right)$, $A(t) = -\frac{(d_1+d_2)}{w\varepsilon_0\varepsilon_1 R(l-x)}$, $B(t) = \frac{\sigma_0 x(d_1+d_2)}{\varepsilon_0\varepsilon_1 R(l-x)}$. The current, voltage and power outputs are respectively,

$$I(t) = \frac{dQ}{dt},\ V(t) = RI(t),\ P(t) = RI(t)^2. \tag{20}$$

References

1. Zheng, X. *Mechanics of Wind-blown Sand Movements*, (Springer, 2009).
2. Redmond, H. E., Dial, K. D. & Thompson, J. E. Light Scattering and Absorption by Wind Blown Dust: Theory, Measurement, and Recent Data. *Aeolian Res*. **2,** 5–26 (2010).
3. Sadiku, M. *Elements of electromagnetics* (*the oxford series in electrical and computer engineering*). (Oxford University Press, 2014).
4. Suzuki, Y. Recent Progress in MEMS Electret Generator for Energy Harvesting. *IEEJ T. Electr. Electr.* **6,** 101–111 (2011).
5. Wang, Z. L. & Song, J. Piezoelectric Nanogenerators based on Zinc Oxide Nanowire Arrays. *Science* **312,** 242–246 (2006).
6. Fan, F. R., Tian, Z. Q. & Wang, Z. L. Flexible Triboelectric Generator. *Nano Energy* **1,** 328–334 (2012).
7. Wang, S. *et al.* Charge-separation Mechanism. *Nano Lett.* **13,** 2226–2233 (2013).
8. Bae, J. *et al.* Flutter-driven Triboelectrification for Harvesting Wind Energy. *Nat. Commun.* **5,** 4929 (2014).
9. Niu, S. *et al.* Theoretical Investigation and Structural Optimization of Single-Electrode Triboelectric Nanogenerators. *Adv. Funct. Mater.* **24,** 3332–3340 (2014).
10. Niu, S. *et al.* A Theoretical Study of Grating Structured Triboelectric Nanogenerators. *Energ. Environ. Sci.* **7,** 2339–2349 (2014).
11. Niu, S. *et al.* Simulation Method for Optimizing the Performance of an Integrated Triboelectric Nanogenerator Energy Harvesting System. *Nano Energy* **8,** 150–156 (2014).
12. Wang, S. *et al.* Maximum Surface Charge Density for Triboelectric Nanogenerators Achieved by Ionized-Air Injection: Methodology and Theoretical Understanding. *Adv. Mater*. **26,** 6720–6728 (2014).
13. Zhu, G., Chen, J., Zhang, T., Jing, Q. & Wang, Z. L. Radial-arrayed Rotary Electrification for High Performance Triboelectric Generator. *Nat. Commun.* **5,** 3426 (2014).
14. Niu, S. *et al.* Theory of Sliding-Mode Triboelectric Nanogenerators. *Adv. Mater.* **25,** 6184–6193 (2013).
15. Lowell, J. & Rose-Innes, A. C. Contact Electrification. *Adv. Phys*. **29,** 947–1023, (1980).
16. Daniel, J. L. & Sankaran, R. M. Contact Electrification of Insulating Materials. *J. Phys. D: Appl. Phys.* **44,** 453001 (2011).
17. Chen, J. *et al.* Harmonic-Resonator-Based Triboelectric Nanogenerator as a Sustainable Power Source and a Self-Powered Active Vibration Sensor. *Adv. Mater.* **25,** 6094–6099 (2013).
18. Wang, S., Lin, L. & Wang, Z. L. Nanoscale Triboelectric-Effect-Enabled Energy Conversion for Sustainably Powering Portable Electronics. *Nano Lett.* **12,** 6339–6346, (2012).
19. Zhu, G. *et al.* Triboelectric-Generator-Driven Pulse Electrodeposition for Micropatterning. *Nano Lett.* **12,** 4960–4965 (2012).
20. Fan, F. R. *et al.* Transparent Triboelectric Nanogenerators and Self-Powered Pressure Sensors Based on Micropatterned Plastic Films. *Nano Lett.* **12,** 3109–3114 (2012).
21. Lin, Z. H. *et al.* Enhanced Triboelectric Nanogenerators and Triboelectric Nanosensor Using Chemically Modified TiO2 Nanomaterials. *ACS nano* **7,** 4554–4560 (2013).
22. Zhu, G. *et al.* Toward Large-Scale Energy Harvesting by a Nanoparticle-Enhanced Triboelectric Nanogenerator. *Nano Lett.* **13,** 847–853 (2013).
23. Zheng, Y. *et al.* An Electrospun Nanowire-based Triboelectric Nanogenerator and its Application in a Fully Self-Powered UV Detector. *Nanoscale* **6,** 7842–7846 (2014).
24. Poppe, T., Blum, J. & Henning, T. Experiments on Collisional Grain Charging of Micron-sized Preplanetary Dust. *Astrophys. J.* **533,** 472–480 (2000).
25. Forward, K. M., Lacks, D. J. & Sankaran, R. M. Triboelectric Charging of Granular Insulator Mixtures Due Solely to Particle−Particle Interactions. *Ind. Eng. Chem. Res.* **48,** 2309–2314 (2008)
26. Hu, W., Xie, L. & Zheng, X. Contact Charging of Silica Glass Particles in a Single Collision. *Appl. Phys. Lett.* **101,** 114107 (2012).
27. Siu, T., Cotton, J., Mattson, G. & Shinbrot, T. Self-sustaining charging of identical colliding particles. *Phys. Rev. E* **89,** 052208 (2014).
28. Bilici, M. A. *et al.* Particle size effects in particle-particle triboelectric charging studied with an integrated fluidized bed and electrostatic separator system. *Rev. Sci. Instrum*. **85,** 103903 (2014).
29. Xie, L., Han, K., Ma, Y. & Zhou, J. An electrification mechanism of sand grains based on the diffuse double layer and Hertz contact theory. *Appl. Phys. Lett.* **103,** 104103 (2013).
30. Pham, R. *et al.* Contact charging between surfaces of identical insulating materials in asymmetric geometries. *J.Electrostat.* **69,** 456–460 (2011).
31. Xie, L. *et al.* An experiment investigation on electrification by collision between chemically identical glass particles. *AIP Conf. Proc.* **1542,** 859–862 (2013).
32. Xie, L., Bao, N. & Zhou, J. Contact electrification by collision of homogenous particles. *J. Appl. Phys.* **113,** 184908 (2013)
33. Wei, X. Y., Zhu, G. & Wang, Z. L. Surface-charge engineering for high-performance triboelectric nanogenerator based on identical electrification materials. *Nano Energy* **10,** 83–89 (2014).
34. Aly, A. A. *et al.* Friction and Wear of Polymer Composites Filled by Nano-Particles: A Review. *World J. Nano Sci. Eng.* **2,** 21006 (2012).
35. Lowell, J. & Truscott, W. S. Triboelectrification of identical insulators. II. Theory and further experiments. *J. Phys. D:Appl. Phys.* **19,** 1281–1298 (1986).
36. Forward, K. M., Lacks, D. J. & Sankaran, R. M. Charge segregation depends on particle size in triboelectrically charged granular materials. *Phys.Rev.Lett.* **102,** 028001 (2009).
37. Kok, J. F. & Lacks, D. J. Electrification of Granular Systems of Identical Insulators. *Phys. Rev. E* **79,** 051304 (2009).
38. Lacks, D. J., Duff, N. & Kumar, S. K. Nonequilibrium Accumulation of Surface Species and Triboelectric Charging in Single Component Particulate Systems. *Phys. Rev. Lett.* **100,** 188305 (2008).
39. Kok, J. F. & Renno, N. O. Electrostatics in Wind-Blown Sand. *Phys. Rev. Lett*. **100,** 014501 (2008).

40. Zheng, X., Zhang, R. & Huang, H. Theoretical Modeling of Relative Humidity on Contact Electrification of Sand Particles. *Sci. Rep.* **4,** 4399 (2014).
41. Fortunato, E., Barquinha, P. & Martins, R. Oxide Semiconductor Thin-Film Transistors: A Review of Recent Advances. *Adv. Mater.* **24,** 2945–2986, (2012).
42. Song, H. Z., Bao, X. M., Li, N. S. & Wu, X. L. Strong Ultraviolet Photoluminescence from Silicon Oxide Films Prepared by Magnetron Sputtering. *Appl. Phys. Lett.* **72,** 356–358, (1998).
43. Thim, G. P., Oliveira, M. A. S., Oliveira, E. D. A. & Melo, F. C. L. Sol–gel Silica Film Preparation from Aqueous Solutions for Corrosion Protection. *J. Non-Cryst. Solids* **273,** 124–128, (2000).
44. Kenyon, A. J., Trwoga, P. F., Federighi, M. & Pitt, C. W. Optical Properties of PECVD Erbium-Doped Silicon-Rich Silica: Evidence for Energy Transfer Between Silicon Microclusters and Erbium Ions. *J. Phys. Condens. Matter* **6,** L319 (1994).
45. De Rouffignac, P., Li, Z. & Gordon, R. G. Sealing Porous Low-k Dielectrics with Silica. Electrochem. *Solid State Lett.* **7,** G306–G308 (2004).
46. Stöber, W., Fink, A. & Bohn, E. Controlled Growth of Monodisperse Silica Spheres in the Micron Size Range. *J. Colloid. Interf. Sci.* **26,** 62–69, (1968).
47. Cui, N. *et al.* High performance sound driven triboelectric nanogenerator for harvesting noise energy. *Nano Energy* **15,** 321–328 (2015).
48. Wang, Z. L., Gao, R. P., Pan, Z. W. & Dai, Z. R. Nano-Scale Mechanics of Nanotubes, Nanowires, and Nanobelts. *Adv. Eng. Mater.* **3,** 657 (2001).
49. Niu, S. *et al.* Theoretical Study of Contact-Mode Triboelectric Nanogenerators as an Effective Power Source. *Energy Environ. Sci.* **6,** 3576–3583 (2013)
50. Love, A. E. H. The Stress Produced in a Semi-Infinite Solid by Pressure on Part of the Boundary. *Philos. T. R. Soc. A* **228,** 377–420 (1929).

Acknowledgements

Thanks Professor Yan Zhang(Lanzhou University, PR. China) for giving good suggestions to improve this study. We are grateful to the National Natural Science Foundation of China(Grand Nos.11302217, 11172285 and 11472259) for financial support.

Author Contributions

W.W. and W.H. designed the TENG with homogenous silica electrification layer. W.H. did the theoretical research. W.W. and W.H. wrote the manuscript. All authors attended discussion with this work and gave suggestions.

Additional Information

Competing financial interests: The authors declare no competing financial interests.

How to cite this article: Hu, W. *et al.* Wind-blown Sand Electrification Inspired Triboelectric Energy Harvesting Based on Homogeneous Inorganic Materials Contact: A Theoretical Study and Prediction. *Sci. Rep.* **6**, 19912; doi: 10.1038/srep19912 (2016).